Ultrafast Radiationless Deactivation of Organic Dyes: Evidence for a Two-State Two-Mode Pathway in Polymethine Cyanines

Adelaida Sanchez-Galvez,[†] Patricia Hunt,[†] Michael A. Robb,*[,†] Massimo Olivucci,*[,‡] Thom Vreven,[†] and H. Bernhard Schlegel[§]

Contribution from the Department of Chemistry, King's College London, Strand, London WC2R 2LS, U.K., Istituto di Chimica Organica, Universitá degli Studi di Siena, via Aldo Moro, I-53100 Siena, Italy, and Department of Chemistry, Wayne State University, Detroit, Michigan 48202

Received November 12, 1999. Revised Manuscript Received January 13, 2000

Abstract: CASSCF quantum chemical calculations (including dynamics) have been used to investigate the ultrafast photoisomerization of three symmetric cyanine dye models of different chain lengths. For the "model" trimethine cyanine, the photochemical isomerization path can be divided into two phases: initial barrierless skeletal stretching coupled with torsional motion and the decay process that takes place in the region of the twisted intramolecular charge-transfer (TICT) minimum state with an adjacent conical intersection. The path is consistent with both biexponential decay of fluorescence without rise time at short wavelengths and the rise time followed by monoexponential decay at long wavelengths observed in time-resolved experiments. For penta- and heptamethine cyanines, the photoisomerization about different C−C bonds is shown to be an activated process, where the torsional reaction path terminates, again, at a TICT state and the decay takes place at a twisted S_1/S_0 conical intersection. In agreement with the experimental results, the activation energies increase with the length of the polymethine chain. In contrast to the differences in the potential energy surface between short and long cyanines, we demonstrate that the excited state evolution of these systems can be understood in terms of the same two-state two-mode model of the reaction coordinate previously reported for the (isoelectronic) retinal protonated Schiff base models.

1. Introduction

Modern femtosecond spectroscopy, in concert with computational chemistry, is beginning to elucidate the mechanism of photoinduced ultrafast chemical reactions in considerable detail.[1,2] These processes provide an efficient route to photochemical production of new chemical species (i.e., photochemistry) and are of basic importance in different photobiological processes such as vision, solar energy storage, and phototropism.[3] The investigation of the reaction path of different photoinduced organic reactions[2] shows that, in general, these processes are nonadiabatic; i.e., the path begins on an electronically excited state of the reactant species and ends on the ground-state energy surface where the product is formed. Further, ultrafast (femtosecond or picosecond) reaction time scales are associated with barrierless (or nearly barrierless) excited-state paths. The central feature of such processes is that at some point along the excited-state reaction coordinate the system enters an extremely efficient decay channel, which takes the form of a conical intersection between the excited- and ground-state potential energy surfaces. After decay at the conical intersection, the system continues its evolution on the ground state to generate a new chemical species (i.e., a photochemical transformation has occurred).

Chart 1

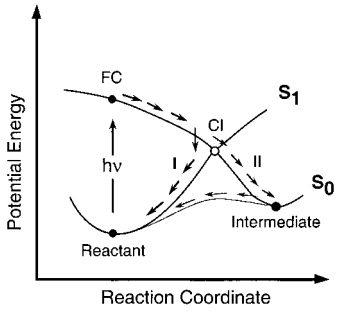

Recent studies also have provided evidence that ultrafast chemical reactions are implicated as the major route *to radiationless deactivation of the excited state of organic species where no net chemical reaction takes place*. This can be accomplished according to two possible, not mutually exclusive, reaction path mechanisms (see Chart 1). In the first mechanism, the evolution toward new chemical species may "abort" at the conical intersection, and the system merely evolves back to the reactant species in a purely photophysical process (process I in Chart 1). Thus, the only result of the process is the *direct* regeneration of the initial ground-state reactant (e.g., the deactivation of singlet $n-\pi^*$ states in azoalkanes[4] and singlet $\pi-\pi^*$ states of short polyenes[5]). In the second mechanism, the excited-state evolution and decay result in the ultrafast produc-

[†] Kings College London.
[‡] Universitá degli Studi di Siena.
[§] Wayne State University.

(1) *Femtochemistry and Femtobiology: Ultrafast Reaction Dynamics at Atomic-Scale Resolution*; Sundstrom, V., Ed.; Nobel Symposium 101, Imperial College Press: Singapore, 1997.

(2) Bernardi, F.; Robb, M. A.; Olivucci, M. *Chem Soc. Rev.* **1996**, *25*, 321.

(3) *CRC Handbook of Organic Photochemistry and Photobiology*, Horspool, W. M., Song, P.-S., Eds.; CRC Press: Boca Raton, FL, 1995.

(4) Nau, W. M.; Greiner, G.; Wall, J.; Rau, H.; Olivucci, M.; Robb, M. A. *Ang. Chem., Int. Ed.* **1998**, *37*, 98. (b) Nau, W. M.; Greiner, G.; Rau, H.; Olivucci, M.; Robb, M. A. *Ber. Bunsen-Ges. Phys. Chem.* **1998**, *102*, 486.

(5) Garavelli, M.; Celani, P.; Bernardi, F.; Robb, M. A.; Olivucci, M. *J. Am. Chem. Soc.* **1997**, *119*, 11487 and references therein.

10.1021/ja993985x CCC: $19.00
Published on Web 03/10/2000

tion of a new ground-state intermediate species or reactant isomers (process II in Chart 1). Then the new ground-state species can revert to the starting form in a thermal process on the ground state (e.g. photochromism; see ref 6 for an example), resulting in the regeneration of the starting material. In general, the nature of the excited-state reaction path and the shape of the potential energy surface in the region of the conical intersection determine which path controls the radiationless deactivation.

An example of the situation where an ultrafast chemical reaction is involved in a radiationless deactivation mechanism of the second type comes from the investigation of biological photoactive proteins such as rhodopsin (the human retina visual pigment) and bacteriorhodopsin (the light-driven bacterial proton pump of halobacteria). The biological activity of these proteins is based on a photocycle whose primary event corresponds to the light-induced *cis*−*trans* isomerization of a retinal protonated Shiff base (PSB) chromophore embedded in the protein. These reactions (see eq 1 for the case of the rhodopsin chromophore)

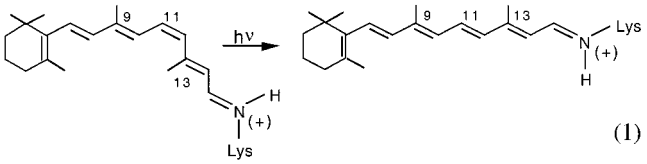

occur on a 200−500 fs time scale[7−11] and thus are among the fastest chemical reactions observed so far. The work of Mathies shows that ultrafast reactions can occur from a nonequilibrated excited-state population (vibrationally unrelaxed),[9b] and a coherent vibrational motion has been observed on the rhodopsin photoproduct.[9c] The results of reaction path computations for different retinal PSB models (see for example refs 12 and 13) show that the ultrafast excited-state evolution of the chromophore can be understood in terms of a two-state two-mode model. In this model, only the ground state (S_0) and the first singlet $\pi-\pi^*$ excited state (S_1) are involved in the reaction. Upon excitation to S_1, the molecule follows a path in which two different vibrational modes are populated sequentially. The first mode is totally symmetric and drives the initially planar system out of the Franck−Condon region through a skeletal stretching. The second vibrational mode is nontotally symmetric and is dominated by torsional motion about one of the central double bonds of the system. This two-mode motion, in turn, leads the system toward a ca. 90° twisted configuration where the S_0 and S_1 potential energy surfaces cross at a conical intersection, thus triggering an extremely efficient $S_1 \rightarrow S_0$ decay. In retinal PSB models this intersection is located right at the bottom of the S_1 energy surface.

While nature provides efficient biological chromophores that utilize ultrafast chemistry, the type of reaction described above can seriously limit the technological exploitation of synthetic organic compounds such as cyanine dyes (see eq 2) where a

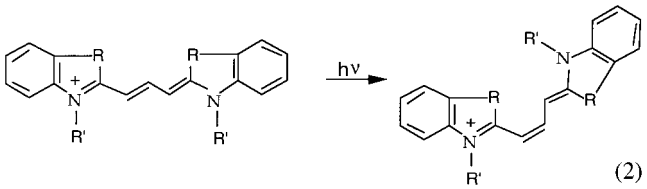

highly fluorescent long-lived singlet $\pi-\pi^*$ state is desirable. Because of their fluorescence properties, cyanine dyes have many uses in technology.[14−22] They have been classically employed as optical sensitizers of silver halide colloids in photographic processes[14−16] and in laser technology.[17,18] More recently new applications have been developed as fluorescent probes in biochemical procedures.[19,20] However, these molecules are characterized by a short excited-state lifetime (5 ps to tens of nanoseconds)[23−28] and, therefore, by a low fluorescence quantum yield in solution (0.06−0.40).[25,29] This low yield is a consequence of an ultrafast nonradiative process which has been attributed to photoinduced *trans*−*cis* isomerization about one

(6) Celani, P.; Bernardi, F.; Robb, M. A., Olivucci, M. *J. Am. Chem. Soc.* **1997**, *119*, 10815.

(7) *The Photophysics and Photochemistry of Retinal Proteins*, Ottolenghi, M., Sheves, M., Eds.; *Isr. J. Chem.* **1995**, *35* (special issue).

(8) (a) Chosrowjan, H.; Mataga, N.; Shibata, Y.; Tachibanaki, S.; Kandori, H.; Shichida, Y.; Okada, T.; Kouyama, T. *J. Am. Chem. Soc.* **1998**, *120*, 9706. (b) Kakitani, T.; Akiyama, R.; Hatano, Y.; Iamamoto, Y.; Shichida, Y.; Verdegem, P.; Lugtemburg, *J. Phys. Chem. B* **1998**, 102, 1334.

(9) (a) Schoenlein, R. W.; Peteanu, L. A.; Mathies, R. A.; Shank, C. V. *Science* **1991**, *254*, 412. (b) Kochendoerfer, G. G.; Mathies, R. A. *J. Phys. Chem.* **1996**, *100*, 14526. (c) Wang, Q.; Schoenlein, R. W.; Peteannu, L. A.; Mathies, R. A.; Shank, C. V. *Science* **1994**, *266*, 422.

(10) (a) Mathies, R. A.; Brito Cruz, C.-H.; Pollard, T. W.; Shank, C. V. *Science* **1988**, *240*, 777. (b) Dobler, J.; Zinth, W.; Kaiser, K.; Oesterhelt, D. *Chem. Phys. Lett.* **1988**, *144*, 215. (c) Kobayashi, T.; Terauchi, M.; Yoshizawa, M.; Taiji, M. *SPIE* **1990**, *144*, 407.

(11) (a) Kandori, H.; Katsuta, Y.; Ito, M., Sasabe, H. *J. Am. Chem. Soc.* **1995**, 117, 2669. (b) Kandori, H.; Sasabe, H. *Chem. Phys. Lett.* **1993**, *216*, 126. (c) Logunov, S. L.; Song, L.; El-Sayed, M. *J. Phys. Chem.* **1996**, *100*, 18586. (d) Hamm, P.; Zurek, M.; Röschinger, Patzelt, H.; Oesterhelt, D.; Zinth, W. *Chem. Phys. Lett.* **1996**, *263*, 613.

(12) (a) Garavelli, M.; Vreven, T.; Celani, P.; Bernardi, F.; Robb, M. A.; Olivucci, M. *J. Am. Chem. Soc.* **1998**, *120*, 1285. (b) Garavelli, M.; Bernardi, F. Olivucci, M.; Vreven, T.; Klein, S.; Celani, P.; Robb, M. A. *Faraday Discuss.* **1998**, *110*, 51. (c) Garavelli, M.; Negri, F.; Olivucci, M. *J. Am. Chem. Soc.* **1999**, *121*, 1023−1029.

(13) Garavelli, M.; Celani, P.; Bernardi, F.; Robb, M. A.; Olivucci, M. *J. Am. Chem. Soc.* **1997**, *119*, 6891−6901.

(14) (a) Naber, A.; Fischer, U. C.; Kirchner, S.; Dziomba, T.; Kollar, G.; Chi, L. F.; Fuchs, H. *J. Phys. Chem. B.* **1999**, *103*, 2709.

(15) Gretchikhine, A.; Schweiter, G.; Van der Auweraer, M.; De Keyzer, R.; Vandenbroucke, D.; De Schryver, F. C. *J. Appl. Phys.* **1999**, *85*, 1283.

(16) (a) Spitler, M. T.; Ehret, A.; Kietzmann, R.; Willig, F. *J. Phys. Chem. B* **1997**, *101*, 2552. (b) Kemnitz, K.; Miller, R. J. D.; Yoshihara, K.; Matsunami, H. J. *J. Phys. Chem.* **1989**, *93*, 6704. (c) Hamilton, J. F. In *The Theory of the Photographic Process*, 4th ed.; James, T. H., Ed.; Macmillan: New York, 1977; pp 235−250.

(17) (a) Fabian, J.; Nakazumi, H.; Matsuoka, M. *Chem. Rev.* **1992**, *92*, 1197−1226. (b) Fleming, G. R. *Chemical Applications of Ultrafast Spectroscopy*; Oxford University Press: New York, 1986.

(18) (a) Kaliteevskaya, E. N.; Razumova, T. K.; Tarnovskii, A. N. *Opt. Spectrosc.* **1999**, *1*, 126−133. (b) Kaschke, M.; Ernsting, N. P.; Valeur, B.; Bourson, J. *J. Phys. Chem.* **1990**, *94*, 5757. (c) Mialocq, J. C.; Goujon, P.; Arvis, M. *J. Chim. Phys. Phys.-Chim. Biol.* **1979**, *76*, 1067. (d) Reynolds, G. A.; Drexhage, K. H. *J. Org. Chem.* **1977**, *42*, 885.

(19) (a) Seifert, J. L.; Connor, R. E.; Kushon, S. A.; Wang, M.; Armitage, B. A. *J. Am. Chem. Soc.* **1999**, *121*, 2987. (b) Tu, O.; Knott, T.; Marsh, M.; Bechtol, K.; Harris, D.; Barker, D.; Bashkin, J. *Nucleic Acids Res.* **1998**, *26*, 2797. (c) Netzel, T. L.; Nafisi, K.; Zhao, M.; Lenhard, J. R.; Johnson, I. *J. Phys. Chem.* **1995**, *99*, 17936.

(20) (a) Nunnally, B. K.; He, H.; Li, L. C.; Tucker, S. A.; McGown, L. B. *Anal. Chem.* **1997**, *69*, 2392. (b) Hung, S. C.; Ju, J. Y.; Mathies, R. A.; Glazer, A. N. *Anal. Biochem.* **1996**, *243*, 15. (c) Krieg, M.; Redmond, R. W. *Photochem. Photobiol.* **1993**, *57*, 472.

(21) Chatterjee, S.; Davis, P. D.; Gottschalk, P.; Kurz, M. E.; Sauerwein, B.; Yang, X.; Schuster, G. B. *J. Am. Chem. Soc.* **1990**, *112*, 6329.

(22) Grieser, F.; Lay, M.; Thistlethwaite, P. J. *J. Phys. Chem.* **1985**, *89*, 2065.

(23) (a) Dempster, D. N.; Morrow, T.; Rankin, R.; Thompson, G. F. *J. Chem. Phys., Faraday Trans. 2* **1972**, *68*, 1479. (b) Berndt, K.; Dürr, H.; Feller, K.-H. *Z. Phys. Chem. Leipzig* **1987**, *268*, 250.

(24) Tarnovsky, A.; Yartsev, A. Private communication.

(25) Levitus, M.; Martín Negrí, R.; Aramendía, P. F. *J. Phys. Chem.* **1995**, *99*, 14231.

(26) Martini, I.; Hartland, G. V. *J. Phys. Chem.* **1996**, *100*, 19764.

(27) Chibisov, A. K.; Zakharova, Görner, H. *J. Chem. Soc., Faraday Trans.* **1996**, *92*, 4917.

(28) Murphy, S.; Sauerwein, B.; Drickamer, H. G.; Schuster, G. B. *J. Phys. Chem.* **1994**, *98*, 13476.

(29) Aramendía, P. F.; Martín Negrí, R.; San Román, E. *J. Phys. Chem.* **1994**, *98*, 3165.

Chart 2. FC Energy Surface Structure

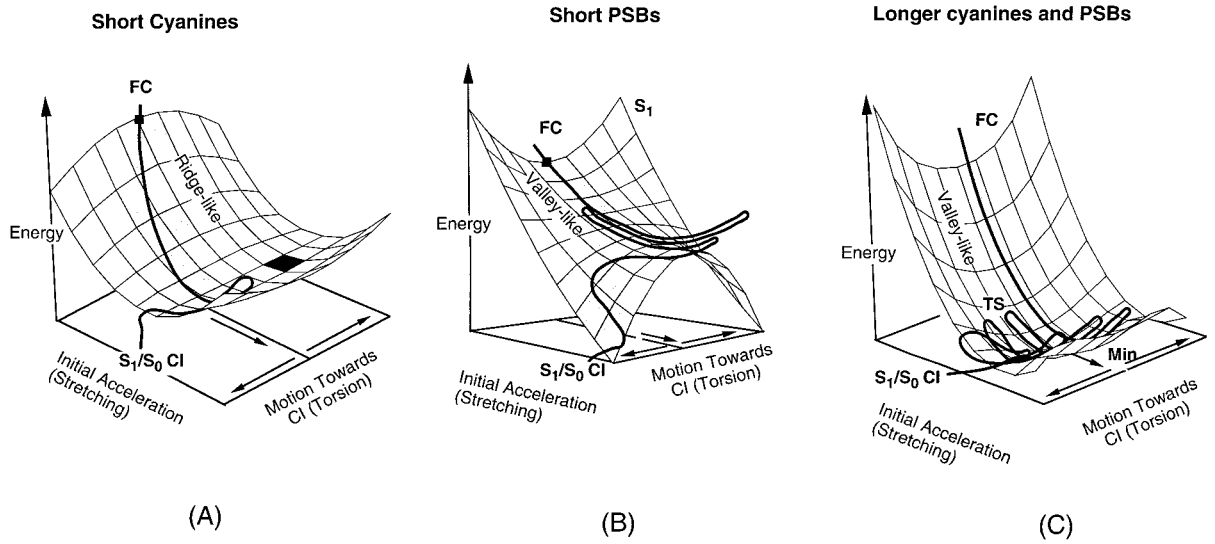

of the C−C bonds of the polymethine chain[29,30] (see eq 2) in analogy with the isoelectronic retinal PSBs (see eq 1). Indeed, the involvement of *trans*−*cis* isomerization in the $S_1 \rightarrow S_0$ deactivation process is consistent with the dramatic fluorescence enhancement obtained by dissolving the dye in viscous solvents, chemical rigidization of the conjugated chain,[31] or adsorbing the dyes in inert surfaces.[32,33]

The challenge to synthetic chemists is to design cyanine dyes where the radiationless *trans*−*cis* isomerization process is "chemically" blocked. The first step in the quest for a solution to this problem is the detailed understanding of the dye deactivation path. In the results to be presented subsequently, we report a computational study of the S_1 reaction pathway and dynamics for three unsubstituted streptocyanines with a three-, five- and seven-unit polymethine chain in isolated conditions. We shall compare this information with the results obtained on the corresponding retinal PSB models that we have documented previously at a similar level of theory.[12,13] The trimethine cyanine NH_2-$(CH)_3$−NH_2^+ is used as a model compound for short-chain cyanines. The reaction pathway and dynamics for this system will be compared with those of the pentadienimminium cation ($C_5H_6NH_2^+$), a "minimal" retinal PSB model.[13] The penta- and heptamethine cyanines are used as models for long polymethine cyanines, and the computational results are compared with those obtained for the longer retinal PSB models[12] heptatrieniminium ($C_7H_8NH_2^+$) and nonatetraeniminium ($C_9H_{10}NH_2^+$) cations.

Our results indicate that, after evolution on the S_1 energy surface, all cyanines are ultimately delivered to S_0 at a ca. 90° twisted S_1/S_0 conical intersection. However, in contrast with the analogous retinal PSB models, the intersection is not located at the bottom of the S_1 energy surface but rather near a fully twisted excited S_1 energy minimum that corresponds to a twisted intramolecular charge transfer[34] (TICT) state of the molecule. Ab initio semiclassical trajectory calculations reveal that, after partial equilibration of the TICT state, the photoexcited cyanine decays to the ground state by populating skeletal asymmetric stretching and NH wagging modes, which modifies the equilibrium geometry toward the conical intersection structure.

In contrast to the differences in the potential energy surface between cyanines and PSB in the region of the conical intersection, the initial excited-state evolution (near the Franck−Condon **FC** point) of the cyanine models considered in this work can be described using the two-state two-mode model reported for the retinal PSBs.[12,13] A detailed analysis of the computed path of the trimethine cyanine indicates that the structure of the S_1 potential energy surface corresponds to that shown Chart 2A. The initial relaxation out of the **FC** point occurs along a barrierless path dominated by skeletal stretching, *strongly coupled* with concurrent torsional deformations of the carbon framework. A similar type of behavior was previously reported for the short PSB model, $C_5H_6NH_2^+$[13] (see Chart 2B). In the PSB model, however, the coupling of the torsional motion does not occur immediately. Rather, a couple of stretching oscillations take place before the onset of the stretching−torsion mixing. As shown in Chart 2B, this delayed mixing of stretching and torsion is due to a change in the topological structure of the S_1 energy surface which exhibits a "valley-like" rather than a "ridge-like" curvature at the **FC** point. In contrast, the S_1 reaction coordinate computed for the longer penta- and heptamethine cyanines suggests that the initial relaxation will be fully dominated by the stretching mode and that the torsional mode will be populated only after partial equilibration at a metastable untwisted intermediate. Thus, the potential energy surface structure given in Chart 2C shows that, for these longer molecules, there is an extended valley-like shape along the stretching coordinate which prevents a fast stretching-torsional coupling. The situation is almost identical to that reported for longer retinal models ($C_7H_8NH_2^+$ and $C_9H_{10}NH_2^+$).[12b]

As we will discuss below, the generalized model illustrated in Chart 2 rationalizes the fact that cyanines with short polymethine chains undergo a barrierless S_1 relaxation while longer chain cyanines decay via slower activated processes. We will see that the surface given in Chart 2A provides a two-dimensional analogue of the empirical model proposed for explaining the behavior of 1,1′-diethyl-4,4′-cyanine in solution.[24,41−43] Similarly the potential energy surface of Chart

(30) Rullière, C. *Chem. Phys. Lett.* **1976**, *43*, 303.
(31) Sczepan, M.; Rettig, W.; Bricks, Y. L.; Slominski, Y. L.; Tolmachev, A. I. *J. Photochem. Photobiol., A* **1999**, *124*, 75−84.
(32) (a) Kawasaki, M.; Inokuma, H. *J. Phys. Chem. B* **1999**, *103*, 1233. (b) Owen, D. J.; VenDerveer, D.; Schuster, G. B. *J. Am. Chem. Soc.* **1998**, *120*, 1705. (c) Ogawa, M.; Kawai, R.; Kuroda, K. *J. Phys. Chem.* **1996**, *100*, 16218.
(33) (a) Botelho do Rego, A. M.; Penedo Pereira, L.; Reis, M. J.; Oliveira, A. S.; Vieira Ferreira, L. F. *Langmuir* **1997**, *13*, 6787. (b) Laguitton-Pasquier, H.; Van der Auweraer, M.; De Schryver, F. C. *Langmuir* **1998**, *14*, 5172.
(34) Rettig, W. *Angew. Chem., Int Ed. Engl.* **1986**, *25*, 971.

2C provides a two-dimensional analogue of Rullière's empirical model[30] which has been proposed to account for the behavior of carbo-, dicarbo-, and tricarbocyanines (cyanines with five, seven, and nine carbon atoms in the polymethine chain, respectively). Our results also explain the results of time-resolved spectroscopic studies which show that both the activation energy and excited-state lifetime increase with the length of the polymethine chain.[15,25−28,35−40] Finally the existence of a TICT intermediate at the bottom of the S_1 energy surface (which can be reached via relaxation from the energy surface given in Chart 2A) seems to provide a realistic explanation for the detectable fluorescence rise time and relatively long decay time constant (4.5−12 ps) observed in 1,1′-diethyl-4,4′-cyanine.[41]

2. Computational Methods

All the MC-SCF energy, gradient, and frequency computations have been carried out using a complete active space (CASSCF) with the 6-31G* basis set as implemented in Gaussian.[44] The choice of active space in our computations is unambiguous. It comprises 6 electrons in 5 π orbitals for the trimethine cyanine (50 configurations), 8 electrons in 7 π orbitals for the pentamethine cyanine (490 configurations), and 10 electrons in 9 π orbitals for the heptamethine cyanine (8001 configurations). The topology of the S_1 potential energy surfaces for these systems has been characterized, optimizing equilibrium structures, transition states, and conical intersections. State-average orbitals were used when the energy gap between the excited state and the ground state becomes small. When state-averaged orbitals were used, the computed gradients were corrected with the CP-MC-SCF correction. The energetics have been corrected at selected critical points by recomputation at the second-order multireference perturbation level of theory using the CASSCF-MP2 algorithm.[45]

We shall subsequently discuss the computation of minimum energy paths (MEPs) from the **FC** point. Since it is not a critical point, we have computed the MEP in two steps. First, we calculate the initial relaxation direction (IRD)[46] from the **FC** point. The IRD is computed by locating the energy minimum on a hyperspherical ((n − 1)-dimensional) cross-section of the n-dimensional potential energy surface (n is the number of vibrational degrees of freedom of the molecule). The hypersphere is centered on the reference point (**FC**), and the IRD is the vector that joins the reference point to the minimum on the hypersphere. Such a vector describes the local steepest descent direction of the energy surface in mass-weighted coordinates in the vicinity of the reference point. The energy minima obtained with this method are referred to as *hypersphere minima*. In a subsequent computation, the MEP is computed using the intrinsic reaction coordinate (IRC) method.[47] When the IRC is to be started from a transition state, the initial direction to be followed is the vibrational coordinate corresponding to the imaginary frequency. In contrast, if the IRC is to be started at a point where the gradient is not zero (e.g., a hypersphere minimum near the **FC** point or near the conical intersection), the IRD vector defines the initial direction to follow.

The vibrational frequencies of stationary points have been computed analytically for tri- and pentamethine cyanines using the methodology available in Gaussian.[44] In the case of the points of an IRC (nonzero gradient), the mass-weighted Hessians have been projected onto a n − 1 space orthogonal to the tangent to the path using the method of the displacement.[46] These vibrational frequencies give information about the shape of the excited potential energy surface orthogonal to the IRC (if it is valley-like or ridge-like). In the case of minima localized with the hypersphere algorithm, the Hessians are projected onto a n − 1 space orthogonal to the IRD vector. The projected vibrational frequencies and the description of the corresponding normal modes along the n − 1 orthogonal space are then obtained by diagonalizing the projected Hessian.

The electronic structure of the molecules has been analyzed using a valence bond (VB) model derived from the CASSCF wave function. A simple VB representation is obtained by localizing the CASSCF active orbitals using the Boys localization procedure. If the active space is complete, then the orbitals will localize onto atomic sites. The corresponding CI expansion gives a VB wave function. The occupancies of each carbon and nitrogen atom are given by the diagonal elements of the first-order density matrix (D_{ii}).[13]

Finally, ab initio "on the fly" semiclassical trajectory calculations[48,49] in the full space of coordinates with surface hopping[50] have been performed for the trimethine cyanine. In this procedure, the gradient and the Hessian need to be computed at each point in the dynamics study, so it is feasible only to run a single representative trajectory from a structure close to the **FC** point. The nonadiabatic surface hop at the crossing is determined by propagating the solutions of the time-dependent (electronic) Schrödinger equation in concert with nuclear propagation. The probability, or relative population of the two states of interest, is used to determine when a hop occurs. In the trajectory discussed subsequently, the criterion for the surface hop proves to be irrelevant since a pure diabatic transition takes place at the surface crossing.

3. Results and Discussion

Trimethine Cyanine Photoisomerization. We shall discuss, in the first part of this section, the excited-state barrierless isomerization of the three-membered cyanine, $NH_2-(CH)_3-NH_2^+$, on S_1. The results for the longer penta- and heptamethine cyanines will be discussed in a subsequent subsection. (We remind the reader that these systems are chosen as "models" for the experimentally studied species which contain fused

(35) Khimenko, V.; Chibisov, A. K.; Görner, H. *J. Phys. Chem. A* **1997**, *101*, 7304.
(36) Tatikolov, A. S.; Dzhulibekov, Kh. S.; Shvedova, L. A.; Kuzmin, V. A.; Ishchenko, A. A. *J. Phys. Chem.* **1995**, *99*, 6525.
(37) Laitinen, E.; Korppi-Tommola, J.; Linnanto, J. *J. Chem. Phys.* **1997**, *107*, 7601.
(38) Voigt, B.; Nowak, F.; Ehlert, J.; Beeken, W. J. D.; Leupold, D.; Sandner, W. *Chem. Phys. Lett.* **1997**, *278*, 380.
(39) Sahyun, M. R.; Serpone, N. V. *J. Phys Chem.* **1997**, *101*, 9877. (b) Khairutdinov, R. F.; Serpone, N. *J. Phys. Chem. B* **1997**, *101*, 2602.
(40) Awad, M. M.; McCarthy, P. K.; Blanchard, G. J. *J. Phys. Chem.* **1994**, *98*, 1454.
(41) Yartsev, A.; Alvarez, J. L.; Åberg, U.; Sundström, V. *Chem. Phys. Lett.* **1995**, *243*, 281.
(42) (a) Åberg, U.; Åkesson, E.; Alvarez, J. L.; Fedchenia, I.; Sundström, V. *Chem. Phys.* **1994**, *183*, 269. (b) Sundström, V.; Åberg, U. *J. Mol. Liq.* **1993**, *57*, 149. (c) Åkesson, E.; Sundström, V.; Gillbro, T. *Chem. Phys. Lett.* **1986**, *106*, 269. (d) Sundström, V.; Gillbro, T. *J. Chem. Phys.* **1982**, *86*, 1788.
(43) Zhang. T.; et al. *Chem. Phys. Lett.* **1998**, *298*, 236.
(44) Gaussian 99, Development Version (Revision B.01): Frisch, M. J.; Trucks, G. W.; Schlegel, H. B.; Scuseria, G. E.; Robb, M. A.; Cheeseman, J. R.; Zakrzewski, V. G.; Montgomery, J. A., Jr.; Stratmann, R. E.; Burant, J. C.; Dapprich, S.; Millam, J. M.; Daniels, A. D.; Kudin, K. N.; Strain, M. C.; Farkas, O.; Tomasi, J.; Barone, V.; Cossi, M.; Cammi, R.; Mennucci, B.; Pomelli, C.; Adamo, C.; Clifford, S.; Ochterski, J.; Petersson, G. A.; Ayala, P. Y.; Cui, Q.; Morokuma, K.; Malick, D. K.; Rabuck, A. D.; Raghavachari, K.; Foresman, J. B.; Ortiz, J. V.; Baboul, A. G.; Cioslowski, J.; Stefanov, B. B.; Liu, G.; Liashenko, A.; Piskorz, P.; Komaromi, I.; Gomperts, R.; Martin, R. L.; Fox, D. J.; Keith, T.; Al-Laham, M. A.; Peng, C. Y.; Nanayakkara, A.; Gonzalez, C.; Challacombe, M.; Gill, P. M. W.; Johnson, B.; Chen, W.; Wong, M. W.; Andres, J. L.; Gonzalez, C.; Head-Gordon, M.; Replogle, E. S.; Pople, J. A., Gaussian, Inc., Pittsburgh, PA, 1998.
(45) (a) McDouall, J. J. W.; Peasley, K.; Robb, M. A. *Chem. Phys. Lett.* **1988**, *148*, 183. (b) Gonzalez, D. Ph.D. Thesis, King's College, University of London, 1999.
(46) Garavelli, M.; Celani, P.; Fato, M.; Bearpark, M. J.; Smith, B. R.; Olivucci, M.; Robb, M. A. *J. Phys. Chem. A* **1997**, *101*, 2023.
(47) (a) Gonzalez. C.; Schlegel, H. B. *J. Chem. Phys.* **1989**, *90*, 2154. (b) Gonzalez, C.; Schlegel, H. B. *J. Phys. Chem.* **1990**, *94*, 5523. (c) Baboul, A. G.; Schlegel, H. B. *J. Chem. Phys.* **1997**, *107*, 9413.
(48) (a) Helkalder, T.; Uggerud, E.; Jensen, H. J. Aa. *Chem. Phys. Lett.* **1990**, *173*, 145. (b) Chen, W.; Hase, W. L.; Schlegel, H. B. *Chem. Phys. Lett.* **1994**, *228*, 436. (c) Warshel, A.; Karplus, M. *Chem. Phys. Lett.* **1975**, *32*, 11.
(49) Vreven, T. Ph.D. Thesis, King's College, University of London, 1998.
(50) Klein, S.; Bearpark, M. J.; Smith, B. R.; Robb, M. A.; Olivucci, M.; Bernardi, F. *Chem. Phys. Lett.* **1998**, *292*, 259.

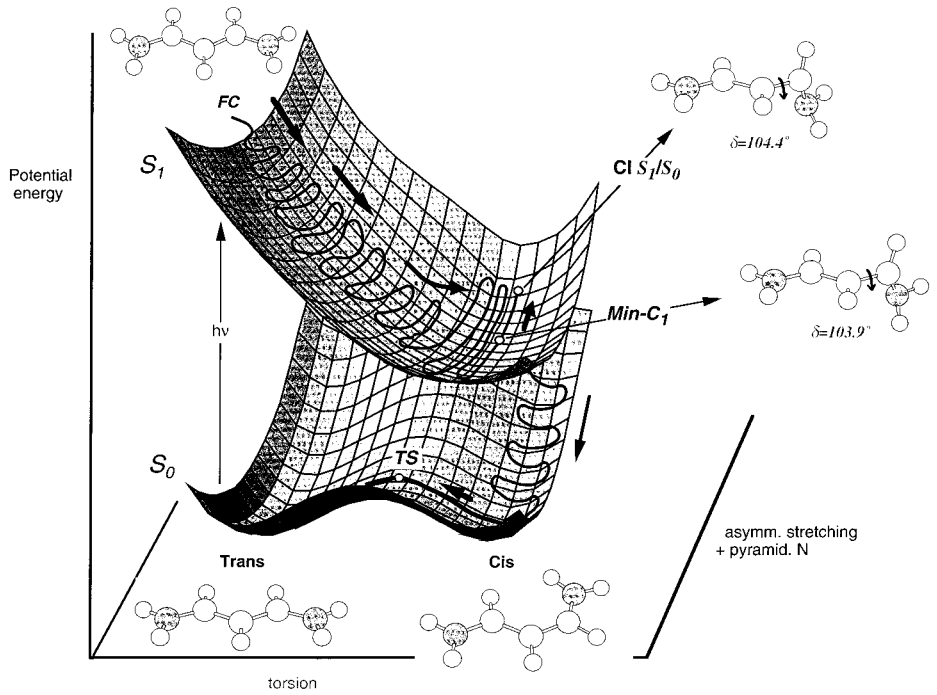

Figure 1. Schematic representation of the structure of the S_1 and S_0 energy surfaces corresponding to the $NH_2-(CH)_3-NH_2^+$ *trans* → *cis* photoisomerization. Two geometric coordinates are used: (a) torsion of the C_2-C_3 and C_3-C_4 bonds and (b) asymmetric stretching coupled with pyramidalization. S_1 and S_0 intersect at a conical intersection (**S_1/S_0 CI**) located near a minimum of the S_1 surface (**Min-C_1**) where the $N_1C_2C_3-C_4N_5$ torsional angle is 104°.

rings). In this paper all geometrical variables are fully optimized, and the nature of the critical points is confirmed by analytic frequency computations and reaction path following methods. We will use the change in dihedral angle of the rotating bond ($N_1C_2-C_3C_4$ or $C_2C_3-C_4N_5$), δ, as a measurement of the reaction coordinate. The value of δ is taken to be 0° for the *trans*-isomer and increases to 180° for the *cis*-isomer so that δ is taken as the reaction coordinate.

It is convenient to begin with an overview of the S_1/S_0 potential surface (using Chart 2A and Figure 1) for trimethine cyanine and then proceed to discuss the more detailed documentation of the salient features of the mechanistic picture. The absorption of a photon generates the **FC** structure on the S_1 energy surface. The analysis of the computed path of the trimethine cyanine model $NH_2-(CH)_3-NH_2^+$ indicates that the initial S_1 relaxation from the **FC** point corresponds to a skeletal symmetric stretching *coupled* with a conrotatory torsion about the two C−C bonds (see Chart 2A). Thus, the torsion is immediately coupled with the stretching coordinate after the excitation to S_1 because the surface in the **FC** region is convex (ridge-like) for the torsional coordinate. This potential surface in the **FC** domain should be compared with the potential surface for the short retinal PSB model, 2-*cis*-$C_5H_6NH_2^+$, illustrated in Chart 2B.[13] The surface topology in the **FC** region of PSB is initially concave (valley-like) with respect to the torsion (see Chart 2B). Only after a partial displacement along the stretching coordinate does the surface become convex at a valley−ridge inflection point, and the torsional motion becomes possible. Thus, the initial motion of the cyanine species can be described by the *two-state two-mode* model[12,13,51] where the two relaxation motions are populated along the reaction coordinate in the region of the **FC** point.

The second stage of the S_1 minimum energy path for the trimethine cyanine is illustrated schematically in Figure 1. After the initial relaxation in the **FC** region, the conrotatory torsion becomes disrotatory, and continues until a TICT minimum, **Min-C_1**, is reached (where the $C_2C_3-C_4N_5$ torsional angle is 104° and the $N_1C_2C_3$ fragment is planar). Adjacent to this S_1 twisted minimum, along an asymmetric skeletal stretching coordinate, a S_1/S_0 conical intersection provides a path for a nonadiabatic evolution toward S_0. The dynamics computations show that several vibrations occur in this skeletal deformation mode before passing through the S_1/S_0 surface crossing. The existence of a minimum in the vicinity of the twisted S_1/S_0 CI represents the main difference with respect to the photochemical behavior of the PSB retinal models, where the torsional motion leads directly to the conical intersection without the intervention of a TICT intermediate.

A. Topology of the Trimethine Cyanine Potential Energy Surface. We now proceed to document the detailed topology of the potential energy surface (shown in Chart 2A for the **FC** region and Figure 1 for the vicinity of the TICT minimum). This documentation will be presented in terms of a set of stationary points optimized on the potential surface (minima, hypersphere minima, and conical intersections) and the corresponding MEP.

The S_0 trimethine cyanine molecule has C_{2v} symmetry. We have located S_1 stationary points with C_{2v}, C_2, and C_1 symmetry (only C_s and C_1 symmetry points were found for the retinal PSB models[12,13]). Both the global minimum (**Min-C_1**) and the lowest energy point on the conical intersection (**S_1/S_0 CI**) have C_1 symmetry. The energies of optimized critical points are collected in Table 1, and the Cartesian coordinates are contained in the Supporting Information. The optimized structures, together with the constrained (C_{2v}, C_2) and unconstrained (C_1) MEP's, provide a detailed picture of the topology of the potential surface which will be confirmed in the dynamics computations that will be discussed subsequently.

Because of the reduction in symmetry ($C_{2v} \rightarrow C_2 \rightarrow C_1$) along the isomerization minimum energy path, the reaction path is

(51) Gonzalez-Luque, R.; Garavelli, M.; Bernardi, F.; Merchan, M. Robb, M. A.; Olivucci, M. To be submitted.

Table 1. CASMP2(6,5)/6-31G* and CASSCF(6,5)/6-31G* Relative Energies at the Stationary Points on the S_1 Surface of Trimethine Cyanine $NH_2-(CH)_3-NH_2^+$ with Respect to the FC C_{2v} Point (kcal·mol^{-1})

structure	CASSCF	CASMP2
FC C_{2v}	0.0	0.0
Min-C_{2v}	−8.2	−7.6
Min-C_2 (state average)	−24.5	−31.5
CI−C_2 (state average)	−22.4	−31.6
Min-C_1 (state average)	−36.9	−39.9
CI S_1/S_0 (state average)	−35.8	−39.7

determined by computing the lowest energy hypersphere minima at different distances from the **FC** point (for details, see the description of the IRD procedure in the Computational Methods). The curvature of the potential energy surface orthogonal to the reaction path at the hypersphere minimum has been determined by evaluating the vibrational frequencies in the subspace orthogonal to the search direction, IRD. These frequencies are also collected in the Supporting Information. The computation of hypersphere minima allows the characterization of the topology of the S_1 potential energy surface in the immediate vicinity of the **FC** structure. Between the **FC** point and 1.00 au, all the lowest energy hypersphere minima have C_2 symmetry. The hypersphere minimum (C_2 symmetry) located at 1.00 au has an imaginary frequency corresponding to asymmetric stretching and conrotatory torsion that lowers the symmetry to C_1. Accordingly, for distances greater than 1.00 au, the lowest energy hypersphere minima all have C_1 symmetry. The C_2 MEP was computed from the hypersphere minimum of C_2 symmetry located at 1.0 au (C_2 symmetry is maintained along this MEP since the motion is dominated by conrotatory torsion), and the full MEP was computed starting at the C_1 hypersphere minimum at 2.0 au.

The totally symmetric skeletal relaxation from the **FC** region is documented via a C_{2v} symmetry constrained MEP which was started from a C_{2v} constrained hypersphere minimum located at 0.5 au from **FC** (this symmetry constrained hypersphere minimum has an imaginary frequency corresponding to conrotatory torsion that lowers the symmetry to C_2).

In the C_{2v} subspace, there is a stationary point (**Min-C_{2v}**) where the bond lengths of the π system are stretched with respect to the **FC** point (Figure 2a). This stationary point lies 8.3 kcal·mol^{-1} below the **FC** structure and is characterized by one imaginary frequency (313i cm^{-1}) corresponding to a conrotatory torsion which lowers the symmetry to C_2. As shown in Figure 2a, the C_{2v} constrained path (*$MEP_{C_{2v}}$*) connects the **FC** structure with the stationary point **Min-C_{2v}**. The potential energy surface topology, represented in the space of the symmetric skeletal deformation (which preserves C_{2v} symmetry) and the conrotatory torsion coordinate (which lifts C_{2v} symmetry), is shown schematically in Figure 2b. For the 0.5 au hypersphere minimum there is an imaginary frequency (410i cm^{-1}) corresponding to a conrotatory double torsion about the C−C bonds. The surface in the **FC** region is convex (ridge-like) along the C_{2v} constrained path. Thus, torsional motion will couple with symmetric stretching immediately after the excitation to S_1. In the retinal model 2-*cis*-$C_5H_6NH_2^+$ (see Chart 2B[13]) the two motions are also coupled. Nevertheless, the surface topology in the **FC** region is slightly different from that of the cyanine. The surface shape changes from valley-like to ridge-like with respect to the torsion, and therefore the initial skeletal stretching and the torsional motion become strongly coupled only after a partial oscillation in the stretching coordinate.

In the C_2 subspace, there is a stationary point (**Min-C_2**) where the two C−C bonds of the polymethine chain are rotated 110.5°

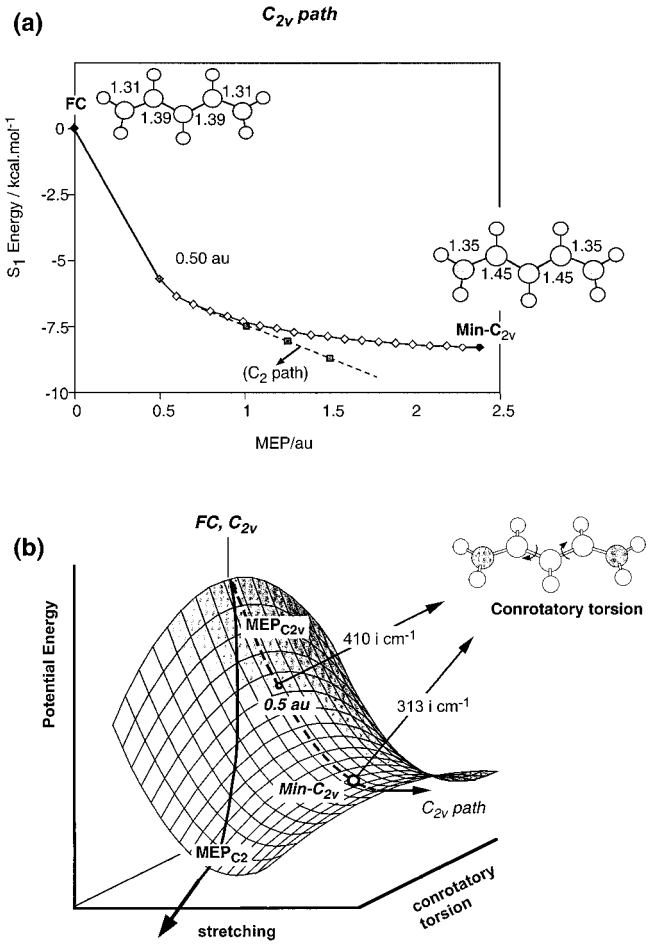

Figure 2. (a) Energy profile along the C_{2v} constrained path (*$MEP_{C_{2v}}$*). The geometrical parameters of the **FC** point and of **Min-C_{2v}** are given in angstroms and degrees. (b) Structure of the S_1 energy surface near the **FC** point in the C_{2v} symmetry space. The *$MEP_{C_{2v}}$* and the *MEP_{C_2}* are indicated by dashed and full lines, respectively. The vibrational frequencies along the *$MEP_{C_{2v}}$* are represented for the 0.5 au hypersphere minimum and for **Min-C_{2v}**.

(see Figure 3). It lies 24.5 kcal·mol^{-1} below the **FC** point with an imaginary frequency (805i cm^{-1}). Adjacent to this minimum, the **CI-C_2** conical intersection lies 2.2 kcal·mol^{-1} higher in energy.

The MEP in the C_2 subspace has been determined from an IRC started from the C_2 1.0 au hypersphere minimum, where the $N_1C_2-C_3C_4$ and $C_2C_3-C_4N_5$ angles are conrotated by ca. 7°. This C_2 constrained path (MEP_{C_2}) is adjacent to the C_{2v} path (see Figure 2a) and connects the **FC** point to the **Min-C_2** as illustrated in Figure 3a. Figure 3b is a schematic representation of the potential energy surface in the space of the conrotatory torsion that preserves C_2 symmetry and a disrotatory coordinate corresponding to the imaginary frequency that lifts the C_2 symmetry. With respect to the conrotatory coordinate, the shape of the surface along the C_2 reaction coordinate changes (see Figure 3b) from valley-like to ridge-like at 1.00 au from the **FC** point. Thus, along the C_2 steepest descent path, the imaginary frequency increases gradually, changing from 129i cm^{-1} at the 1.00 au hypersphere minimum to 805i cm^{-1} at **Min-C_2**. Therefore, the curvature of the ridge becomes larger along the *MEP_{C_2}* path. The motion driving the molecule out of the ridge at **Min-C_2** corresponds to a combination of disrotatory torsion and stretching coordinates. However, at the 1.00 au point, where the C_2 path is abandoned, the 129i cm^{-1} imaginary frequency is best described as an *asymmetric stretching coupled*

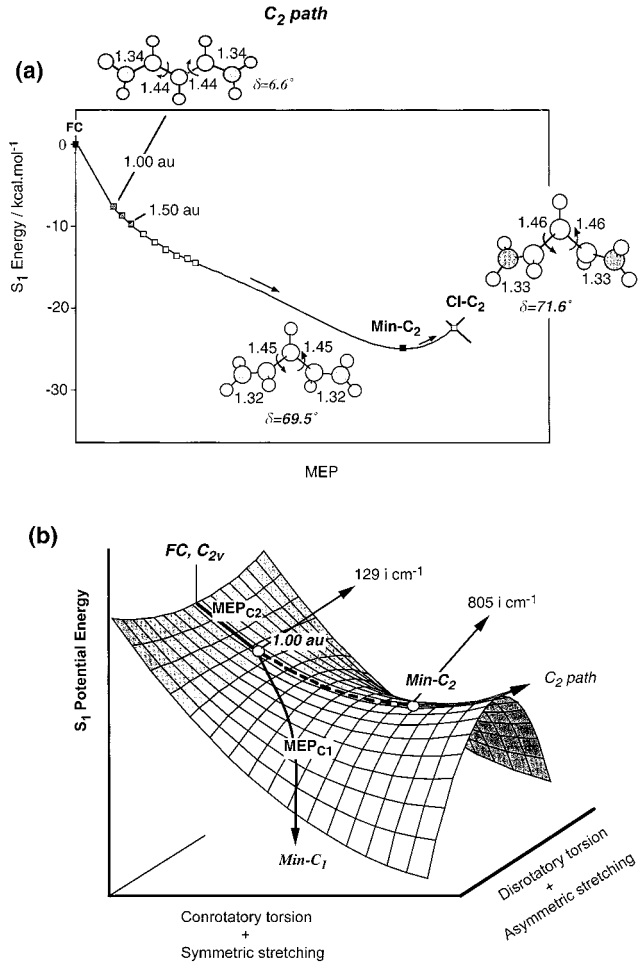

Figure 3. (a) Energy profile along the C_2 constrained path (MEP_{C_2}). The geometrical parameters are given in angstroms and degrees. (b) Structure of the S_1 energy surface near the **FC** point in the C_2 symmetry space. The constrained MEP_{C_2} and the unconstrained MEP_{C_1} are indicated by dashed and full lines, respectively. The vibrational frequencies along the MEP_{C_2} are represented for the 1.00 au hypersphere minimum and for **Min-C_2**.

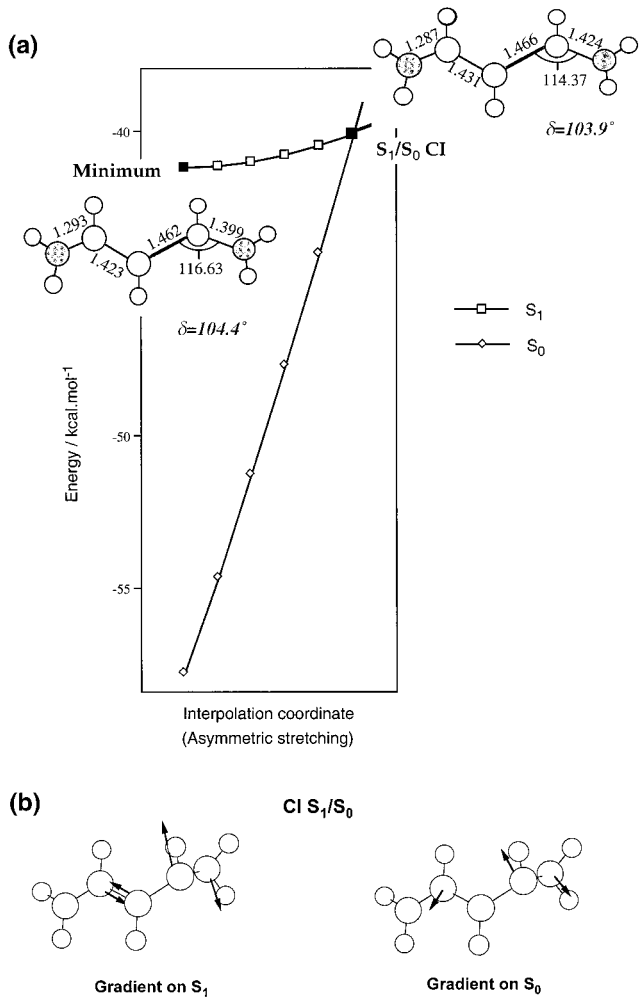

Figure 4. (a) Optimized molecular structures (geometrical parameters in angstroms and degrees) of **Min-C_1** and **S_1/S_0 CI** and the interpolation coordinate between both structures. This figure is related to Figure 1, where the reaction coordinate connecting them was illustrated as an asymmetric stretching coupled with pyramidalization. (b) Gradients of the S_1 and S_0 energy surfaces at the conical intersection **S_1/S_0 CI**.

with conrotatory torsion. In summary, Figure 3b shows that, after excitation of the C_{2v} ground-state structure to S_1, the C_2 conrotatory torsion will be initiated in addition to the skeletal deformation, since the shape of the surface near the **FC** point is valley-like in the conrotatory coordinate. At the 1.00 au C_2 symmetry hypersphere minimum (7° twisted), the shape of the surface becomes convex in the disrotatory coordinate and the C_2 path will be abandoned.

The search for stationary points *without symmetry constraint* yields an absolute minimum, **Min-C_1**. This minimum is ~104° twisted about the C_3-C_4 bond. Adjacent to it, the lowest energy conical intersection (**S_1/S_0 CI**), which provides the decay channel to the ground state, has been optimized. As illustrated in Figure 4a, the main geometric change between the **S_1/S_0 CI** and the **Min-C_1** consists of asymmetric skeletal stretching and NH_2 pyramidalization.

The full unconstrained relaxation path (MEP_{C_1}), shown in Figure 5, *corresponds to the minimum energy path for the photoisomerization of the trimethine cyanine*. It begins at the **FC** point and terminates at the twisted **Min-C_1** equilibrium structure. The details of the geometric changes along the full reaction path are shown in parts ii and iii of Figure 5. As noted previously, because of the reduction in symmetry, the reaction path was determined initially by computing the lowest energy hypersphere minima for different distances and computing their vibrational frequencies (see Supporting Information).

From the **FC** point to 1.00 au, because the lowest energy hypersphere minima have C_2 symmetry, both the unconstrained (MEP_{C_1}) and the C_2 constrained (MEP_{C_2}) paths follow the same descent line: a *skeletal symmetric stretching with a component of conrotatory double torsion* (see bond distances in Figure 5iii). The C_2 path is abandoned from 1.00 au since the shape of the surface in the C_2 subspace changes at 1.00 au from valley-like to ridge-like (see Figure 3b). The motion followed by the molecule at this distance corresponds to its imaginary frequency motion (129i cm^{-1}), which is a *conrotatory double torsion coupled with asymmetric stretching*. Hence, from 1.00 au, the symmetry is reduced to C_1 due to the asymmetric stretching, but the two rotating bonds (δ_1 and δ_2) continue to twist in a conrotatory way (Figure 5ii).

At ca. 2.00 au (20° twisted structure), the lowest energy hypersphere minimum has C_1 symmetry. From this point, the MEP has been computed by following the steepest descent coordinate (IRC) in the usual fashion. The conrotatory torsion is strongly coupled with an asymmetric stretching ($\Delta R_2 \approx -\Delta R_3$ in Figure 5ii) of the central C−C bonds in the polymethine chain, while the terminal N−C bonds (R_1 and R_4) remain practically unchanged. Figure 5ii shows that beyond the 3.90

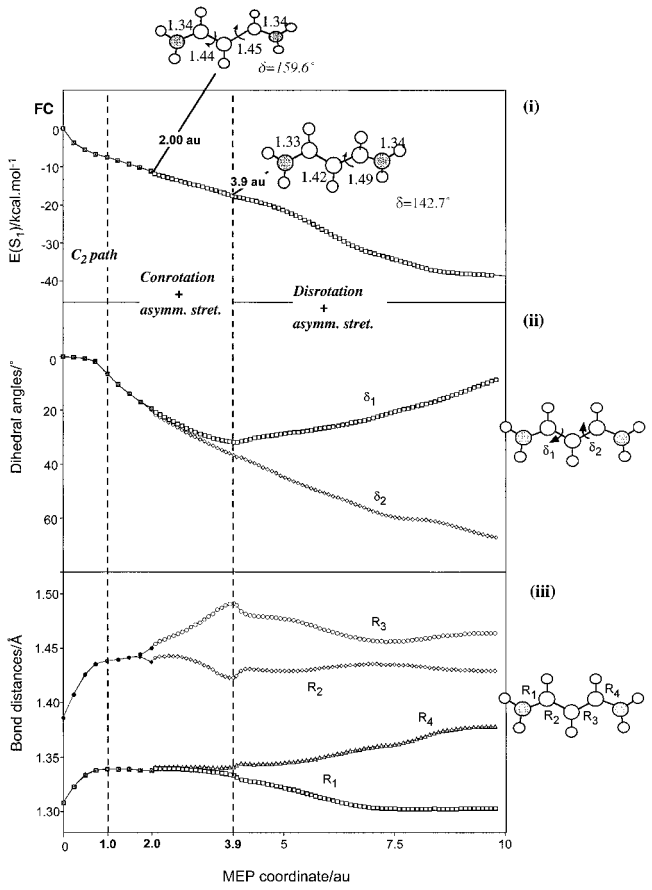

Figure 5. Reaction coordinate analysis along the unconstrained relaxation path (MEP_{C_1}), which corresponds to the minimum energy path for the *trans* → *cis* photoisomerization of the trimethine cyanine. It connects the **FC** point to the absolute minimum **Min-C_1**. (i) Evolution of the S_1 potential energy. (ii) Dihedral angles corresponding to the rotation about the C−C bonds ($\delta_1 = N_1C_2-C_3C_4$ and $\delta_2 = C_2C_3-C_4N_5$). (iii) Bond distances (R_1-R_4) of the polymethine chain.

au point, the reaction coordinate changes. The conrotatory double torsion no longer occurs, and *disrotatory torsion* ($\Delta\delta_1 \approx -\Delta\delta_2$) starts to take place. This disrotatory motion, coupled with asymmetric stretching and $N_1C_2C_3$ fragment planarization, continues until the **Min-C_1** absolute minimum is reached. The lowest vibrational frequencies at the **Min-C_1** minimum of the S_1 surface are 96 and 208 cm^{-1}, indicating that the minimum well is very flat. Close to this stationary point, the **S_1/S_0 CI** conical intersection lies slightly higher in energy and has a geometry very similar to that of the minimum (see Figure 4a).

The geometrical distortion connecting **Min-C_1** and **S_1/S_0 CI** is mainly an asymmetric stretching. The CAS/6-31G* energy difference between **Min-C_1** and the **S_1/S_0 CI** conical intersection is 1.1 kcal·mol^{-1}, decreasing to 0.6 kcal·mol^{-1} with CASMP2. The energy is plotted along an interpolation coordinate between both structures in Figure 4a and illustrates that the S_1 surface is very flat and the S_0 surface is very steep. This topological feature is also reflected in the magnitude of the gradients at the conical intersection, shown in Figure 4b. The S_1 gradient at the **S_1/S_0 CI** conical intersection is almost 0, while the gradient of the S_0 surface is fairly large and corresponds to the torsion about the C_3-C_4 bond of the polymethine chain.

B. Electronic Changes along the Reaction Coordinate. The charge redistribution along the reaction coordinate merits further discussion. As mentioned in the Computational Methods, a simple VB representation is obtained by localizing the CASSCF active orbitals onto atomic sites. The charges on each atom can

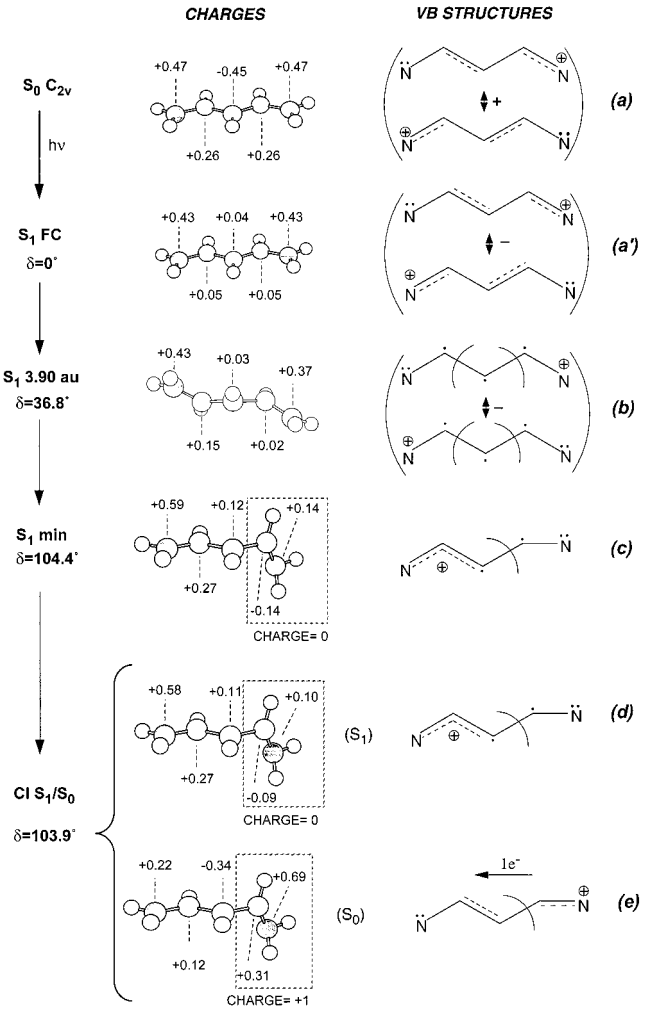

Figure 6. Evolution of the charge distribution (left) for selected points along the minimum energy path (MEP_{C_1}) for the *trans* → *cis* photoisomerization of $NH_2-(CH)_3-NH_2^+$. The corresponding resonance structures obtained with the valence bond analysis of the CASSCF wave function are represented on the right.

then be computed as the difference between the number of "valence" electrons (2 for N, 1 for C) and electron occupancies (values of the diagonal elements of the first-order density matrix, D_{ii}, obtained in the localized orbital basis). The results of the VB analysis along the photoisomerization reaction path are illustrated in Figure 6. Here we present the evolution of the electronic structure, which acts as the driving force for the relaxation of the molecule on the S_1 excited state and provides a qualitative explanation about the behavior of the molecule.

The trimethine cyanine system has 6 electrons distributed in 5 π orbitals. At the **FC** geometry, the ground state is described by the bonding (+) combination of the VB structures shown in Figure 6a, and in S_1 one has the antibonding (−) combination shown in Figure 6a′. Comparing the charges shown in part a and a′ of Figure 6, it is clear that in both structures each nitrogen has 1.5 electrons and the three-carbon chain has 3 electrons: in S_0 the central carbon has a negative charge of ca. 0.5 electrons which results from equal charge transfer from the adjacent carbons, while in S_1 the C atoms are essentially neutral.

The initial S_1 relaxation direction from the **FC** point corresponds to an immediate conrotatory torsion coupled with symmetric skeletal relaxation (see Figure 5). This motion is driven by the bond weakening associated with the antibonding (−) combination of VB structures shown in Figure 6a′. This feature also explains why the **FC** regions for the $NH_2-(CH)_3-$

NH_2^+ system (Figure 2b) and for the retinal model 2-*cis*-C_5H_6-NH_2^+ [13] (Chart 2B) have a slightly different topology. Unlike the cyanine, the initial skeletal stretching coordinate for the retinal model 2-*cis*-$C_5H_6NH_2^+$ is not immediately coupled with the torsional motion because at the **FC** point of this system, the central CC skeletal bond retains some double bond character and is initially stable (valley-like) with respect to the twisting motion.[13]

In Figure 5 it can be seen that conrotatory torsion $\Delta\delta_1 = \Delta\delta_2$ coupled with asymmetric stretching ($\Delta r_2 = -\Delta r_3$) takes place from 1.00 to 3.90 au along the MEP. The electronic change associated with this motion consists of the uncoupling of the π-electrons in the two rotating bonds (see the 3.9 au structure of Figure 6b). At 3.90 au the conrotatory torsion becomes disrotatory ($\Delta\delta_1 = -\Delta\delta_2$ in Figure 5ii). This new motion is driven by the resonance stabilization shown in the VB structure 6c, which initiates the asymmetric stretching and the planarization of the $N_1-C_2-C_3$ skeleton and in turn causes disrotatory torsion. This effect is also the origin of the valley−ridge inflection point on the C_2 constrained MEP shown in Figure 3b, where the asymmetric stretching begins. This motion breaks the C_2 symmetry along two equivalent deformations due to resonance stabilization of the $N_1-C_2-C_3$ (or the $C_2-C_4-N_5$) fragment.

Thus, the final phase of the relaxation motion becomes a single torsion about the C_3-C_4 bond, causing a homolytic cleavage of this π bond. There is a concomitant change in the charge distribution changes and the positive charge shift toward the planar $N_1-C_2-C_3$ fragment. Ultimately, at the TICT minimum **Min-C_1**, this fragment is positively charged with 3 π electrons delocalized in an allylic electronic structure (Figure 6c), and with 3 electrons in the twisted C_4N_5 fragment, which is formally uncharged. Therefore **Min-C_1** is a biradical. The same TICT electronic structure characterizes the adjacent conical intersection on the S_1 surface (Figure 6d). Thus, as proposed in other theoretical studies,[52−56] the decay to the ground state occurs by reverse charge transfer (Figure 6e). At the conical intersection for S_0, the $N_1-C_2-C_3$ fragment of the conical intersection becomes neutral, while the C_4N_5 fragment becomes positively charged. Therefore, passing through **S_1/S_0 CI** involves one electron transfer from S_1 to S_0. This is only possible at the critical geometry where the electron affinity of the planar fragment $(N_1-C_2-C_3)^+$ is equal to the ionization potential of the C_4N_5 fragment. Although the TICT **Min-C_1** and **S_1/S_0 CI** have similar geometries, the structural difference is large enough that the charge transfer can only happen at the critical geometry of the conical intersection. The same mechanism is seen in retinal PSB model systems.[12,13]

C. Reaction Path on the Ground State. The **S_1/S_0 CI** conical intersection provides a channel for the ultimate decay of the molecule to the ground state. Neither **Min-C_1** nor the **S_1/S_0 CI** conical intersection are exactly perpendicular structures, but rather are ca. 105° twisted. Thus, as shown in Figure 1, the conical intersection lies on the "*cis*-side" of the potential energy surface. Therefore, it is expected that the reaction on the ground state will lead to the *cis*-isomer, rather than to the *trans*-isomer.[53d] To demonstrate this, we have determined the reaction coordinate on the ground state starting from the **S_1/S_0 CI** conical intersection. For this purpose, we have calculated the possible initial relaxation directions from **S_1/S_0 CI**. Our results show that there is only one S_0 minimum energy reaction path. It leads to the ground-state *cis*-isomer and has been characterized by optimizing a hypersphere minimum located at 1.00 au from the **S_1/S_0 CI** conical intersection. This structure is then used as a starting point to compute the steepest descent path (IRC), which terminates at the *cis*-isomer geometry. Of course, these computations have used the lowest point on the conical intersection as a reference point. The system may decay at any point on the conical intersection that is energetically accessible. Thus, while decay from the lowest point on the conical intersection leads to the *cis*-isomer, decay at higher energies may produce the *trans*-species.

The *cis*-isomer on the ground state can revert to the *trans*-form via *thermal back-isomerization* on S_0 toward the *trans*-isomer,[55,56b] shown in Figure 1. The reaction coordinate corresponds to the torsion about the C_3-C_4 bond, where the value of δ changes from 180° for the *cis*-isomer to 0° for the *trans*-isomer. The CASMP2(6,5)/6-31G* energy barrier computed for the *cis* → *trans* isomerization on S_0 is 12.1 kcal·mol^{-1} (experimental values[55] for symmetric substituted carbocyanines range from 11 to 13 kcal·mol^{-1}). The rotation angle is δ = 95.6 cm^{-1}, and the imaginary frequency is 289 cm^{-1}. The Cartesian coordinates corresponding to the hypersphere minimum and the TS (*cis* → *trans*) are contained in the Supporting Information.

D. Dynamics Simulation. The static picture of the relaxation dynamics of S_1 trimethine cyanine just discussed can be augmented by means of ab initio semiclassical trajectory calculations in the full space of coordinates. The trajectory has been started at a point on the minimum energy path MEP_{C_1} where the C_2 symmetry has already been abandoned. This trajectory describes in turn the final part of the relaxation process (far away from the **FC** region), thus providing a detailed description of the decay process in the vicinity of the conical intersection. Of course, a single trajectory cannot yield real dynamic information. Rather it serves to illustrate how the energy can flow into modes orthogonal to the reaction coordinate (MEP) and provides some information on those vibrations that prompt the nonadiabatic process that occurs near the TICT minimum on S_1. The results of the trajectory calculation are represented in Figure 7.

We have illustrated the evolution along the trajectory by plotting torsion about the $C_2C_3-C_4N_5$ bond (δ in Figure 7ii). The initial point (the hypersphere minimum located at 3.00 au from the **FC** point) is 25° twisted and is located in the region where the C_2 path has been fully abandoned. The first 50 fs of the trajectory is dominated by conrotatory torsion. It then inverts, and a disrotatory torsion takes place for a short period of time (between 50 and 70 fs) until the molecule is 104° twisted. This feature was already predicted by the topology of the surface and the computed MEP. The rotational motion about the $N_1C_2C_3-C_4N_5$ bond ceases after 70 fs, and the system reaches the domain of the flat **Min-C_1** well (see δ in Figure 7ii). Here the molecule begins to execute large amplitude deformations that do not have any torsional component (the rotating bond does not change; see Figure 7ii). These large amplitude deformations from the **Min-C_1** toward **S_1/S_0 CI** correspond to

(52) (a) Kosower, E. M. *Faraday Discuss.* **1982**, *74*, 161. (b) Kosower, E. M. *Acc. Chem. Res.* **1982**, *15*, 259.

(53) (a) Baraldi, I.; Carnevali, A.; Caselli, M.; Momicchioli, F.; Ponterini, G.; Berthier, G. *J. Mol. Struct.: THEOCHEM* **1995**, *330*, 403. (b) Momicchioli, F.; Baraldi, I.; Berthier, G. *Chem. Phys.* **1988**, *123*, 103. (c) Caselli, M.; Momicchioli, F.; Ponterini, G. *Chem. Phys. Lett.* **1993**, *216*, 41. (d) Momicchioli, F.; Baraldi, I.; Ponterini, G.; Berthier, G. *Spectrochim. Acta* **1990**, *46A*, 775.

(54) Dekhtyar, M.; Rettig, W.; Rozenbaum, V. *J. Photochem., Photobiol., A* **1999**, *120*, 75.

(55) Rodriguez, J.; Scherlis, D.; Estrin, D.; Aramendia, P. F.; Martin Negri, R. *J. Phys. Chem. A* **1997**, *101*, 6998.

(56) (a) Dietz, F.; Rentsch, S. *Chem. Phys.* **1985**, *96*, 145. (b) Krossner, T.; Dietz, F. *Chem. Phys.* **1991**, *153*, 63.

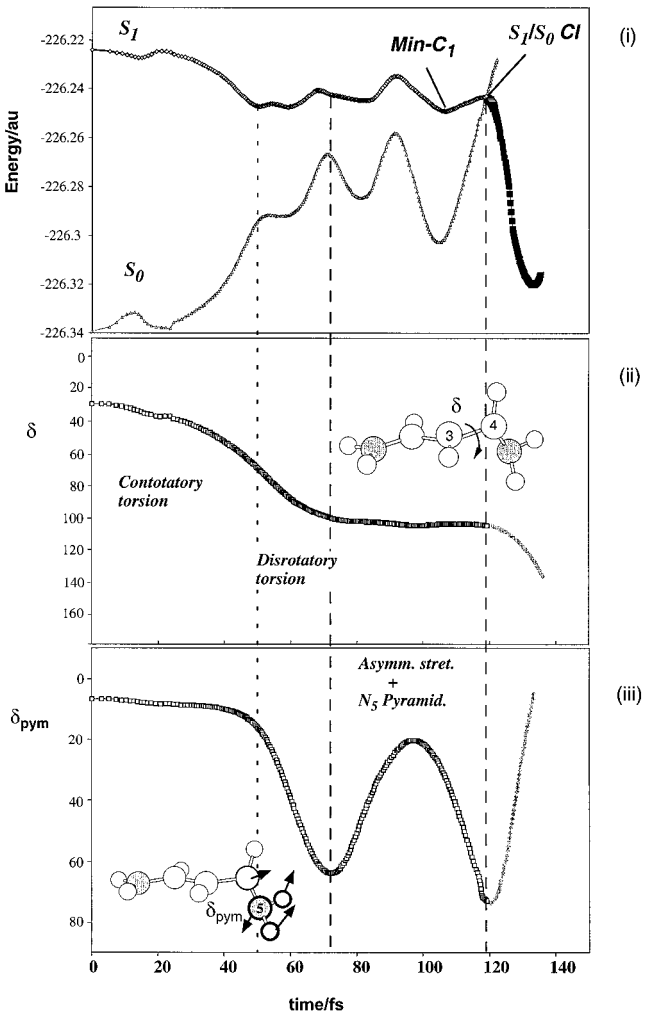

Figure 7. Time evolution along the S_1 trajectory for the *trans* → *cis* photoisomerization of the trimethine cyanine: (i) energy of the S_1 and S_0 states, which become degenerate at **S_1/S_0 CI**, (ii) dihedral angle corresponding to the rotation about the C_3-C_4 bond of the polymethine chain, and (iii) dihedral angle corresponding to the pyramidalization of the terminal nitrogen, N_5. This motion is strongly coupled with the asymmetric stretching of the polymethine chain.

a *skeletal stretching mode coupled with a strong pyramidalization of the terminal nitrogen* N_5 (δ_{pym} plotted in Figure 7iii). The nature of this oscillatory motion can be explained in terms of the vibrational motion corresponding to the two lowest frequencies of **Min-C_1**, which are skeletal asymmetric stretching (96 cm^{-1}) and pyramidalization of the terminal nitrogen (208 cm^{-1}). The system oscillates in this flat region for 50 fs (between 70 and 120 fs) and then passes through the S_1/S_0 conical intersection. The S_1/S_0 hop does not occur exactly at the **S_1/S_0 CI** previously optimized (which is the minimum of the $(n-2)$ dimensional crossing), but at a slightly higher energy (3.9 kcal·mol^{-1} above the minimum).

The analysis of S_1 and S_0 probabilities in the hopping region, shown in Figure 8, indicates that the hop occurs almost diabatically. The hop occurs on the side of the *cis*-isomer (at the hop geometry the molecule is twisted by ca. 105°). The propagation of the trajectory on the ground state leads to the *cis*-isomer. In summary, the trajectory indicates that, after the system has evolved from the **FC** region, the motion is dominated by torsion, leading to a twisted minimum. After several oscillations in the minimum in a skeletal deformation coordinate, the system undergoes a simple diabatic surface hop to the ground state (see Figure 1). This is in contrast to the retinal 2-*cis*-C_5H_6-NH_2^+ model system,[13] where the torsional motion takes the system directly through the conical intersection.

E. Comparison with Experimental Data. We conclude this section with comparison with recent spectroscopic observations. Before doing this, however, we need a brief "aside" to discuss the implications of the fact that ultrafast reactions occur from a nonequilibrated (vibrationally unrelaxed) excited-state population,[9b] where the system is not thermalized.

From theoretical calculations, we are looking for regions of the potential energy surface that may cause a trajectory to perform a small number of oscillations, so that the system remains in that region long enough to be detected experimentally via a transient signal, a transient absorption, fluorescence, or stimulated emission. (Note, by transient, we do not mean thermalized; the reactions occur too quickly for this.) Thus, the presence of a very flat region of the potential energy surface or the presence of a small barrier can be assumed to provide conditions for the creation of such transient species. For example, a system may remain for a few oscillations in the region near the conical intersection because of the presence of a barrier to the conical intersection. The system has to distribute the acquired vibrational energy into the right mode to reach the effective decay point. (Indeed, our trajectory computations demonstrate that a system remains for a few vibrations in the region near the conical intersection for this reason.) Thus, comparison with experimental results is only possible from a "mechanistic point of view". By this we mean the presence or absence (experimentally) of the transient signal. Quantitative comparison of time scales is impossible at our level of theory, since we are dealing with oversimplified models.

The trimethine cyanine has been used as a model for the 1,1′-diethyl-4,4′-cyanine (1144-C cyanine, Chart 3a). For the 1144-C molecule, the relaxation dynamics of different regions on the S_1 surface have been investigated by fluorescence up-conversion spectroscopy, where the fluorescence decays were measured at different wavelengths in propanol and hexanol.[41] For short-wavelength detection, it is possible to observe the region close to the **FC** point. In this high-energy spectral window, the biexponential decay of the fluorescence ($t_1 \approx 1$ ps, $t_2 \approx 4.5$ ps for propanol) and the pronounced solvent dependence of the lifetimes suggest that the wave packet motion corresponds to a barrierless rotational motion. No rise time is detected for this system at short wavelengths. However, Zhong et al.[57] report that for bacteriorhodopsin there is an exceedingly short rise time (faster than 30 fs) when measuring at short wavelengths (**FC** region), which is indicative of the existence of a short-lived transient species undergoing skeletal vibrations with no torsional intermediate (i.e., the system is transported from the observation "window" very quickly along a skeletal deformation coordinate). *Thus, for barrierless trans−cis photoisomerizations, the observation of a short or nonexistent rise time at short wavelengths is the signature of transient species along the skeletal deformation coordinate in the **FC** region.*

However, when the fluorescence is measured at long wavelengths, the decay is no longer biexponential. Rather, one can observe an ultrafast rise time, followed by a slower monoexponential decay (that takes place with a time constant of 4.5 ps in propanol). The so-called rise time is a highly nonexponential initial part of the decay where the fluorescence intensity remains constant for a short period of time (400−700 fs). In the previously proposed potential energy curve for 1144-C,[18,28−30]

(57) Zhong, Q.; Ruhman, S.; Ottolenghi, M.; Sheves, M.; Friedman, N.; Atkinson, G. H.; Delaney, J. K. *J. Am. Chem. Soc.* **1996**, *118*, 12828−12829.

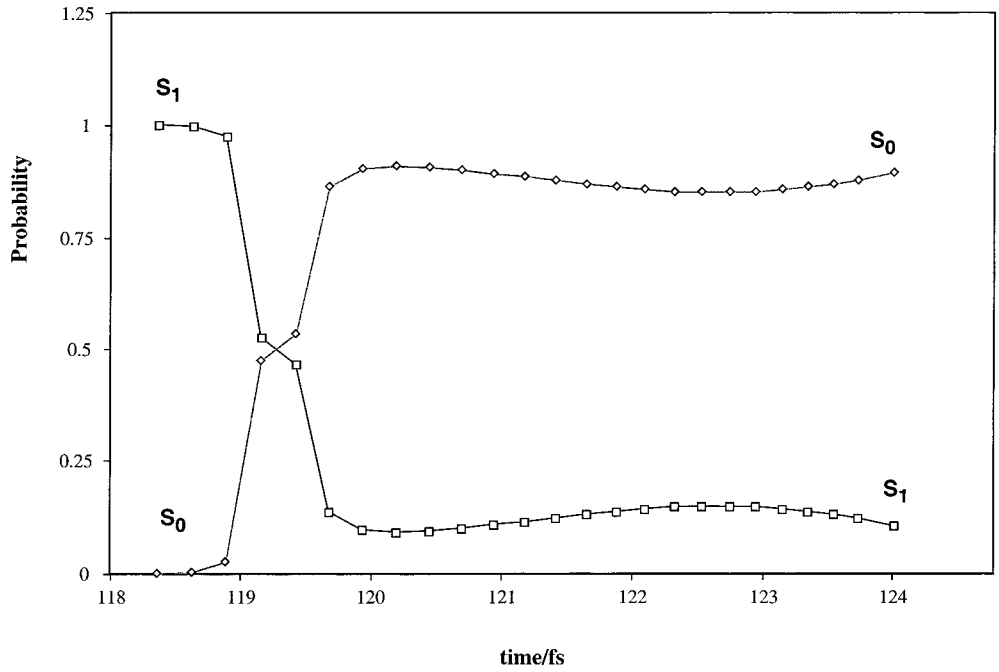

Figure 8. S_1 and S_0 probabilities in the hopping region of the trajectory.

Chart 3

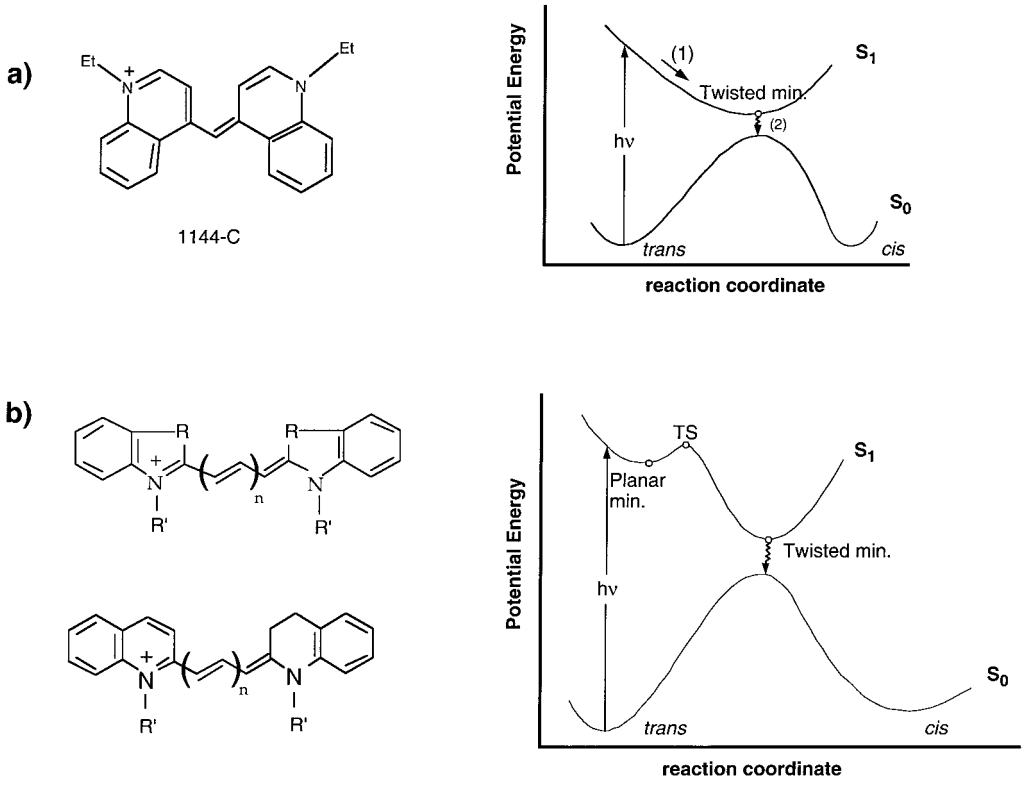

the isomerization reaction coordinate (process 1 of Chart 3a) is followed by an internal conversion $S_1 \rightarrow S_0$ from the perpendicular minimum[41] (process 2 of Chart 3a). The monoexponential decay measured at long wavelength has been attributed to this internal conversion. In comparison with the ultrafast disappearance of the excited population in bacteriorhodopsin[11] (500 fs), the internal conversion $S_1 \rightarrow S_0$ in 1144-C is significantly slower (4.5−12 ps). This slow process, in turn, allows the detection of the rise time of the fluorescence.

The computed potential energy surface topology in the **FC** region coupled with the results with ab initio semiclassical dynamics computations near the region of the TICT minimum provides a *tentative* rationalization for these experimental results. We have demonstrated that the first relaxation process on S_1 is barrierless (see Chart 2A and Figures 2 and 3) and corresponds to skeletal stretching coupled with torsion. This feature can be related to the fluorescence decay *at short detection wavelengths* (region close to the **FC**). Thus, a part of the population remains near the FC region long enough to be observed. From our results it is clear that the reaction path to the TICT minimum breaks symmetry twice, so one may have a slow IVR with consequent increased lifetime in the high-energy region. We can speculate

that the biexponential decay observed implies that two nonradiative processes contribute to the disappearance of the excited population. According to our results, these two processes are (i) the barrierless relaxation, from the **FC** structure, toward the TICT S_1 minimum (**Min-C_1**), followed at longer time by decay through the conical intersection, and (ii) the direct $S_1 \rightarrow S_0$ radiationless decay of the molecules that lie in the "fringe" of the initial vibrational wave packet of the **FC** region, and have the right geometry to enter the S_1/S_0 crossing region. The last point is rather subtle and needs some further discussion. The S_1/S_0 conical intersection is in fact a $(n - 2)$-dimensional hyperline. The molecule can decay anywhere in the crossing region. We have, in fact, computed two points on the hyperline: the S_1/S_0 conical intersection with C_2 symmetry (**CI-C_2**), 31 kcal mol^{-1} below the **FC** point, and the 103° twisted conical intersection (**S_1/S_0 CI**), 40 kcal mol^{-1} below the **FC** point (see Table 1). Thus, the process ii is just the result of radiationless decay at geometries well above the lowest energy conical intersection point **S_1/S_0 CI**. This hypothesis is now under testing via molecular dynamics computations in the **FC** region.

The observed rise time (transient) and the slow monoexponential decay detected *at long detection wavelengths* (i.e., close to the TICT minimum) are closely related to the presence of the flat part of the S_1 potential energy surface near the S_1 minimum (see Figure 1). The shallow coordinate corresponds to a nonreactive motion (stretching coupled with pyramidalization). Thus, the system may oscillate in the shallow part of the TICT minimum, and this can tentatively be related to the appearance of the rise time before the actual decay of the fluorescence takes place. Thus, an observed rise time at long wavelengths is an indication of a nonreactive motion during several vibrational periods in the S_1 minimum well. Finally, the monoexponential character of this decay is justified by the presence of the **S_1/S_0 CI** conical intersection, which lies higher in energy than the minimum. Decay is thus an activated process which withdraws the excited-state population in a fully efficient way toward the ground state.

Finally, our results suggest that, in principle, coherent oscillatory[9c] motion of the hot ground-state product population can be predicted for our short model trimethine cyanine, following direct decay to the ground state. However, partial vibrational relaxation in the TICT well may make the observation of coherent oscillation difficult (although it is difficult to predict the effect of the heterocyclic substituents on this process).

S_1 Energy Surfaces for Longer Polymethine Cyanines. An important question to be answered is how the length of the polymethine chain affects the photophysics of the cyanines. For this purpose, we have studied the pentamethine and heptamethine cyanines, where the chain length is extended by one and two ethylene units, respectively. These molecules may undergo competitive *trans*−*cis* photoisomerization about several C−C bonds of the polymethine chain. In contrast to the barrierless MEP of the trimethine cyanine, it has been found that all the possible isomerizations correspond to activated processes. For these two molecules we have only carried out a topological study of the surface, given that the ab initio dynamics calculations are prohibitively expensive. We use the same convention for the isomerization coordinate, which will be represented by the change in the dihedral angle, δ, corresponding to the rotating C−C bond from $\delta = 0°$ (*trans*) to $\delta = 180°$ (*cis*).

The photoisomerization of these two long streptocyanines can also be understood in terms of the two-state two-mode photochemical model.[12,13,51] Unlike the short trimethine cyanine model, the stretching modes and the torsional modes are completely uncoupled (i.e., sequentially populated) along the S_1 coordinate. The first populated mode is symmetric skeletal relaxation that leads to a C_{2v} minimum, and the second one is a twisting motion (isomerization). Therefore, the topology of the S_1 PES changes substantially with respect to the trimethine cyanine, and it is similar to the long retinal models[12] (see Chart 2C). The reason for this is simply the influence of a longer polymethine chain, in which the stability of the π system is enhanced by electronic delocalization. Thus, in contrast to the trimethine, the S_1 surface in the vicinity of the **FC** point is valley-like with respect to any possible twisting, and the initial relaxation follows a totally symmetric skeletal deformation mode.

A. Pentamethine Cyanine. This molecule may undergo *trans*−*cis* photoisomerization about the C_2-C_3 and C_3-C_4 bonds. Figure 9 illustrates the energy profiles computed for each, and the activation energies are collected in Table 2. The equilibration of the excited population from the **FC** region consists of a *skeletal relaxation* which leads to an all-*trans* C_{2v} minimum structure, which lies 3.15 kcal·mol^{-1} below the **FC** point. At the CASSCF(8,7)/6-31G* level, the energy barriers are 0.58 kcal·mol^{-1} for the rotation about the C_3-C_4 bond and 1.45 kcal·mol^{-1} for the C_2-C_3 bond (these values decrease to 0.18 and 0.56 kcal·mol^{-1} with multireference MP2 correction). These activation energies are very low, and the processes can be considered as nearly barrierless. IRC calculations computed from each transition state have proved that the minimum energy reaction path leads to a twisted structure. Each MEP terminates near a S_1/S_0 real crossing (conical intersection), which corresponds to a ca. 99° twisted geometry for the C_3-C_4 rotation and a ca. 106° twisted geometry for the C_2-C_3 one. No attempt was made to determine the exact structure of the minimum near the end of the MEP. For comparison with the trimethine cyanine, we have also studied the C_2 conrotatory double torsion about the central C_3-C_4 and C_4-C_5 bonds. A transition state located 13.8 kcal·mol^{-1} above the C_{2v} minimum indicates that this process is negligible in comparison with the single torsion about the C−C bonds.

The changes in the electronic structure along the reaction coordinate are similar to those discussed previously. The twisting about a C−C bond results in the formation of two decoupled π fragments with an odd and an even number of carbon atoms, respectively. When the conical intersections are reached, the positive charge is completely localized on the fragment with an odd number of carbon atoms, which is $NH_2-(CH)-$ for the C_2-C_3 rotation and $NH_2-(CH)-(CH)-(CH)-$ for the C_3-C_4 rotation (data not shown).

B. Heptamethine Cyanine. The skeletal relaxation from the **FC** region leads to an all-*trans* C_{2v} minimum that lies 1.55 kcal·mol^{-1} below the **FC** point. The topology of the S_1 energy surface is equivalent to the one presented in Figure 9 for pentamethine cyanine. Three potential isomerization paths corresponding to the different C−C bonds (C_2-C_3, C_3-C_4, and C_4-C_5) can take place from the C_{2v} minimum. Given the size of this cation, a detailed characterization of the surface was not attempted, and we have limited ourselves to optimization of the minima, transition states, and conical intersection. The height of the activation barriers strongly depends on the position of the C−C bond that rotates (Table 2). The tendency is that the closer the C−C bond is to the amino group, the larger is the activation energy. It increases from 2.22 kcal·mol^{-1} at position C_4-C_5 to 7.72 kcal·mol^{-1} at position C_2-C_3. Thus, the lowest energy path for the photoisomerization of the heptamethine cyanine is associated with the rotation about the central bond

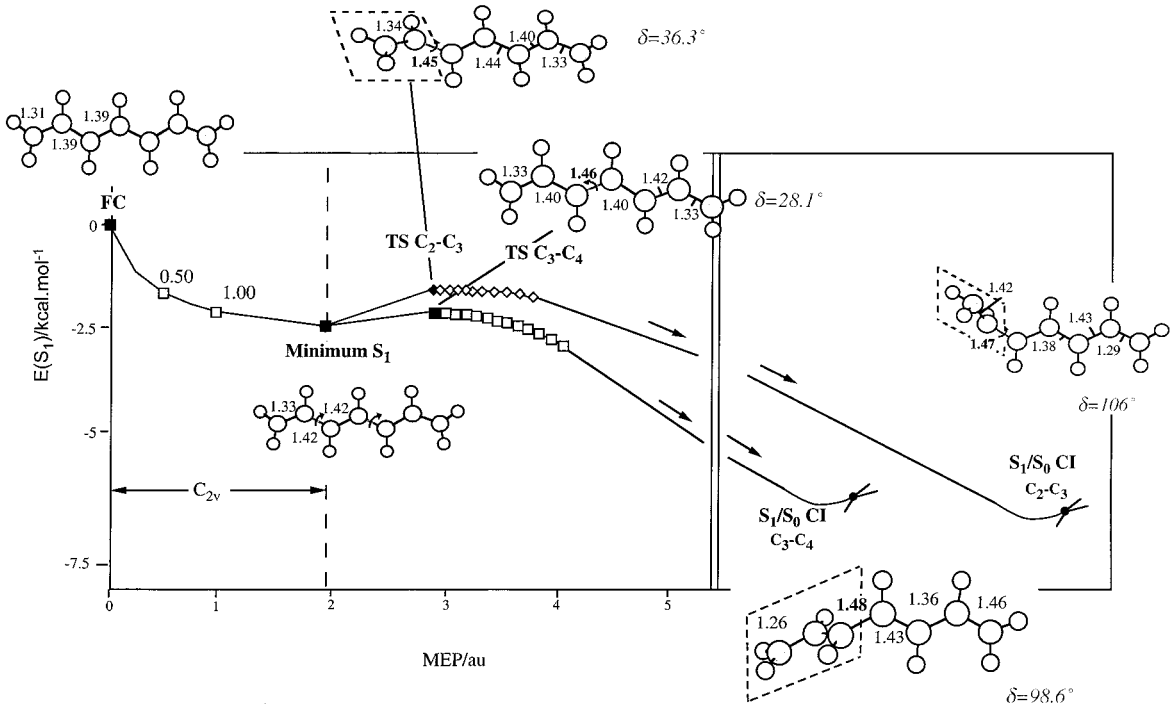

Figure 9. Energy profiles along two photoisomerization paths for pentamethine cyanine, corresponding to the rotation about the C_2-C_3 and C_3-C_4 bonds, respectively. The geometrical parameters are given in angstroms and degrees. Both paths are activated and connect the **FC** point with the corresponding conical intersections.

Table 2. CASMP2/6-31G* and CASSCF/6-31G* Activation Energies (kcal·mol^{-1}) for the *trans*−*cis* Photoisomerization about Several C−C Bonds in the Three Unsubstituted Streptocyanines (Tri, Penta, and Hepta) Studied in This Work

	C_2-C_3		C_3-C_4		C_4-C_5	
	CASCSF	CASMP2	CASCSF	CASMP2	CASCSF	CASMP2
trimethine cyanine $[NH_2\text{-}(CH)_3-NH_2]^+$	barrierless					
pentamethine cyanine$[NH_2\text{-}(CH)_5-NH_2]^+$	1.45	0.56	0.58	0.18		
heptamethine cyanine $[NH_2\text{-}(CH)_7-NH_2]^+$	8.92	7.72	6.98	4.63	3.79	2.22

of the polymethine chain. The rotation about the favored C_4-C_5 bond drives the molecule toward a twisted minimum which lies 4.5 kcal·mol^{-1} below the transition state. An adjacent S_1/S_0 conical intersection with a geometry very similar to the minimum provides the nonadiabatic route to the ground-state isomers. The geometries of the transition state, minimum, and S_1/S_0 conical intersection corresponding to the C_4-C_5 isomerization are collected in Figure 10.

4. Conclusions

The ultrafast photoisomerization of symmetric cyanines has been investigated using the CASSCF method for three model (tri, penta, and hepta) unsubstituted streptocyanines. We have compared the results with the retinal PSB models previously documented.[12,13]

The computed minimum energy paths and the dynamics results for trimethine cyanine suggest that the experimental data can be rationalized by dividing the relaxation process into two phases: the initial relaxation in the **FC** region of the surface and the decay process that takes place in the region of the TICT minimum. The theoretical results for the **FC** region indicate that the initial motion on the potential surface corresponds to skeletal stretching coupled with torsion and that the two-state two-mode model proposed for PSB[12,13,51] remains valid. While for the short-wavelength experimental data no rise time can be detected for the trimethine cyanine, an extremely short rise time is detected in bacteriorhodopsin.[57] Thus, the observation of a short or nonexistent rise time appears to be the "signature" of a transient species undergoing essentially skeletal vibration with some coupled torsional motion. The theoretical results in the region of the TICT minimum can be tentatively associated with the observed longer rise time at long wavelengths. This spectrocopic feature is the signature of the motion that corresponds to torsion, leading to the TICT minimum. Of course, in the 1144-C system studied experimentally, the TICT structure may be more stable than in our model system because of the stabilization of the fused rings.

The experimental data for trimethine cyanine is usually interpreted using a single-mode model[30] (see Chart 3a). This model suggests that, after excitation in the $\pi-\pi^*$ band, the molecule reaches a minimum along a torsional coordinate and then undergoes radiationless deactivation to the ground state from the TICT minimum. This picture must be compared with both Chart 2 (for the **FC** region) and Figure 1 (for the TICT minimum region) that constitute the new model that arises from our computations. It is clear that that a two-state two-mode model is essential for the **FC** region and that both torsion and skeletal stretching are required to reach the region of the TICT minimum. Further, the decay to the ground state occurs not at the TICT minimum, as suggested in Chart 3a, but rather from a conical intersection that lies slightly higher in energy. Thus, the observed relatively long time (4.5−12 ps) for internal conversion[41] arises not because of the large gap shown in Chart 3a, but rather because a funnel for fast decay (the conical intersection) lies adjacent to but at higher energy than the twisted minimum. The decay process is thus activated, and many

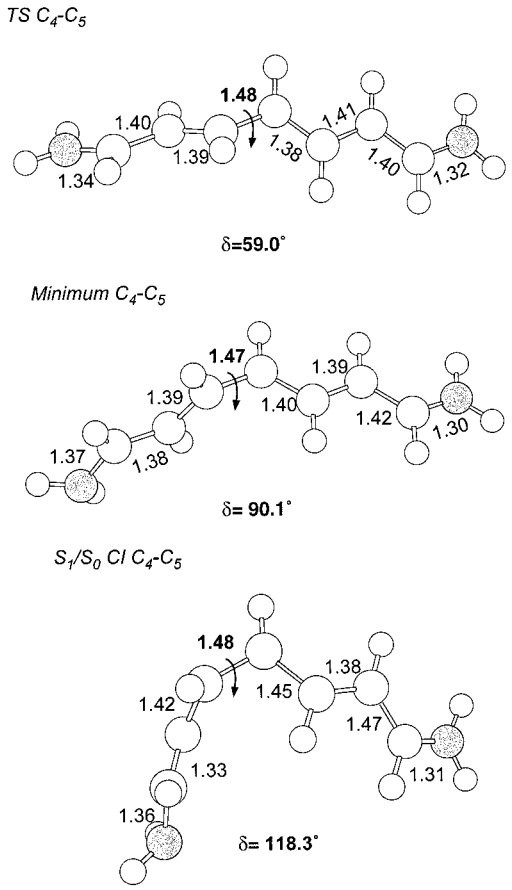

Figure 10. Optimized molecular structures for relevant points along the photoisomerization path about the central bond (C_4-C_5) of the heptamethine cyanine (bonds in angstroms and angles in degrees).

oscillations can take place in the well adjacent to the conical intersection before decay occurs.

Unlike the short cyanines, photoisomerization of long-chain cyanines (Chart 3b) is an activated process. Time-resolved spectroscopic studies[15,25−28,35−40] show that the activation energy and the excited-state lifetime increase with the length of the polymethine chain. Rullière's model,[24] shown in Chart 3b, suggests that, after excitation in the $\pi-\pi^*$ band, the molecule reaches a minimum and then undergoes the *trans−cis* isomerization, passing through a transition state. This torsional motion then leads to a perpendicular minimum that decays to the ground state by internal conversion. Our results confirm that the photoisomerization for the cyanine models with a long polymethine chain is consistent with the two-state two-mode model shown in Chart 2C and is similar to the longer retinal models. The barrier for S_1 torsion is lowest for bonds furthest removed from the N atoms. It has also been demonstrated that the activation energy for the *trans−cis* isomerization of streptocyanines increases with the length of the polymethine chain.

We are currently studying the dynamics from the Franck−Condon region to clarify the connection with experiment in more detail. The synthesis and photophysics of our computed models (especially the long chain cyanines which behave in a fashion similar to that of our PSB models) would be an interesting experimental target.

Acknowledgment. All computations were carried out on an IBM-SP2 funded jointly by IBM-UK and HEFCE (U.K.). This research has been supported in part by the SERC (U.K.) under Grant Number GR/L99623 and by an EU TMR network grant (ERB 4061 PL95 1290, Quantum Chemistry for the Excited State). A.S.G. is grateful to the Ministerio de Educación y Cultura of Spain for her postdoctoral grant (EX 97 24247391, Formación de Personal Investigador en el Extranjero).

Supporting Information Available: Table S1, CASMP2 and CASSCF absolute energies at CASSCF(6,5)/6-31G* optimized geometries for trimethine cyanine $NH_2-(CH)_3-NH_2^+$,) Table S2, CASMP2 and CASSCF absolute energies at CASSCF-(8,7)/6-31G* optimized geometries for pentamethine cyanine $NH_2-(CH)_5-NH_2^+$,) Table S3, CASMP2 and CASSCF absolute energies at CASSCF(8,7)/6-31G* optimized geometries for heptamethine cyanine $NH_2-(CH)_7-NH_2^+$, and tables of Cartesian coordinates (*XYZ*) for the MC-SCF/6-31G* optimized structures (PDF). This material is available free of charge via the Internet at http://pubs.acs.org.

JA993985X